Microchimica Acta (2023) 190:259
https://doi.org/10.1007/s00604-023-05796-x

ORIGINAL PAPER

Fluorescence detection of dopamine based on the peroxidase-like activity of Fe_3O_4-MWCNTs@Hemin

Feijian Xiao[1] · Yijie Wang[1] · Qiulan Li[1] · Dezhi Yang[1] · Yaling Yang[1]

Received: 10 February 2023 / Accepted: 11 April 2023 / Published online: 12 June 2023

Abstract

A novel Fe_3O_4-MWCNTs@Hemin nanocomposite was synthesized using hemin and Fe_3O_4 with multi-walled carbon nanotubes (MWCNTs) by one-step hydrothermal methods. The as-prepared Fe_3O_4-MWCNTs@Hemin nanocomposites exhibited excellent peroxidase-like activities in the activation of H_2O_2. The mechanisms, kinetics, and catalytic performances of Fe_3O_4-MWCNTs@Hemin were systematically studied. Fe_3O_4-MWCNTs@Hemin can oxidize dopamine (DA) to dopaquinone in the presence of H_2O_2, and the intermediate products dopaquinone can further react with β-naphthol to generate a highly fluorescent derivative at 415 nm excitation wavelength. Therefore, an innovative fluorescence platform for the detection of DA was developed. The fluorescence intensity increased linearly with DA concentration in the range 0.33 to 107 μM, with a low detection limit of 0.14 μM. Due to the excellent activity, substrate universality, fast response, high selectivity, and sensitivity of Fe_3O_4-MWCNTs@Hemin, the proposed fluorescence method was used to analyze complex biological blood samples with a satisfactory result. It demonstrated the significant potential for developing effective and dependable fluorescent analytical platforms for preserving human health.

Keywords Nanozymes · Fe_3O_4-MWCNTs · Dopamine · Hemin · Fluorescence detection

Introduction

Dopamine (DA) is an essential excitatory neurotransmitter for intercellular communication in central and cardiovascular systems, which plays an important role in maintaining the balance of various physiological functions, signal transduction, and hormone balance [1, 2]. DA exists in the urine, brain, and blood, abnormal level of DA can be closely bound up with serious neurological disorders, including Parkinson's disease, depression, senile dementia, schizophrenia, and Alzheimer's disease [3, 4]. Therefore, trace detection method of DA has important practical significance for human health and therapy or prevention of various diseases [5]. Up to now, numerous analytical technologies have been explored for DA detection, such as high-performance liquid chromatography (HPLC) [6], mass spectrometry [7], electrochemical methods, and colorimetry [8]. Amongst them, fluorescence analysis method is widely exploited owing to its high sensitivity, good selectivity, and fast response [9, 10]. However, DA has no fluorescence by itself, and fluorescence detection is mainly based on the inhibition of DA on fluorescent substances, such as fluorescent carbon dots [11, 12].

Nanozymes were a kind of artificial mimic enzyme, which has attracted a lot of attention in the research due to its unique spatial structure and abundant active sites, easy preparation, low cost, and adjustable activity [13]. After Fe_3O_4 NPs had good POD-like activity had been reported by Gao and his colleagues [14], a variety of nanomaterials have been exploited successively and have different enzyme activities [15]. Some metal oxides, carbon materials, precious metals, and metal–organic skeletons were developed for fluorescence detection, electrochemical methods, and colorimetric methods. Due to their superior characteristics, Fe_3O_4 nanoparticles are well-known and used in a variety of biological separation, drug administration, magnetic resonance imaging, and biocatalytic applications. The most successful Fe_3O_4-based nanozymes for simulating peroxidase have been found to be those that could produce hydroxyl radical (·OH) by Fenton oxidation. However, Fe_3O_4

✉ Yaling Yang
yilyil8@163.com

1 Faculty of Life Science and Technology, Kunming University of Science and Technology, Kunming 650500, Yunnan, China

nanoparticles have some limitations, such as their poor water solubility, ease of aggregation, and big particle size, which have a significant impact on their catalytic activity [16]. Therefore, several ligands including other metal, organic frame, and inorganic substance are used for assembling Fe_3O_4 to compensate for shortcomings in catalytic activities, which has been discovered were GO@Fe_3O_4, Fe_3O_4@Pt, and so on [17, 18].

Hemin is an iron protoporphyrin compound, which is an active cofactor of heme-proteins, such as cytochromes, peroxidase (HRP), myoglobin, and hemoglobin [19]. It may acquire peroxide-like activity comparable to the POD, which as the POD active site, several biomimetic nano-enzymes have been produced by the inclusion of hemin in diverse materials to gain numerous enzymes and unique biological proteins [15, 20]. It is delighted to find appropriate support that may serve as stabilizers and ligands for Fe ions at the same time to synergistically maximize the catalytic activity of hemin [21]. Chemical synthesis of hemin-graphene hybrid nanosheets was employed to create a platform for detecting phenols because of the POD-like activity [22]. Single-wall carbon nanotubes (SWCNTs) and multi-wall carbon nanotubes (MWCNTs) are the two forms of carbon nanotubes. MWCNTs have drawn the attention of many researchers because of their superior electrical and mechanical properties [23, 24]. Due to the exceptional qualities, MWCNTs are becoming frequently used for creating magnetic adsorbents, which also could be used to increase oxide dispersion because of their stability and great adsorption capacity [25].

In this study, a one-step hydrothermal process was used to synthesize the Fe_3O_4-MWCNTs@Hemin compound and showed greater POD mimic activities. Subsequently, DA could be oxidized by the Fe_3O_4-MWCNTs@Hemin with the activation of H_2O_2 due to the synergism of POD-like, which the oxidative products dopaquinone could further react with β-naphthol (β-NAP) and associated with strong fluorescence. Based on this, a rapid, highly sensitive, and selectivity fluorescence sensor was developed for DA detection.

Experimental

Valuation POD-like activity of Fe_3O_4-MWCNTs@Hemin

The POD-like activity was measured using TMB, ABTS, OPD, and DA a chromogenic substrate. Catalytic assay experiments were carried out in acetate buffer (pH 4.0) in the presence of H_2O_2 and at room temperature. After the reactions, the color formation was monitored absorbance value. To estimate the reaction kinetics of Fe_3O_4-MWCNTs@Hemin, the initial reaction rates of these solutions were measured. The Michaelis–Menten constant (K_m) and the maximal velocity (V_{max}) were obtained by the Michaelis–Menten equation:

$$v = \frac{V_{max} + [S]}{K_m + [S]}$$

Fluorometric detection of DA

A fluorescent platform was built based on Fe_3O_4-MWCNTs@Hemin POD-like activity for the DA detection. Briefly, different concentration of DA was added in acetic acid-sodium acetate buffer (pH = 4.0), then the solution was added to 50 μL H_2O_2, 400 μL β-NAP, and 20 μL Fe_3O_4-MWCNTs@Hemin were added to reach an overall volume of 3 mL. Each solution was mixed and reacted at 30°C water bath for 20 min. Each solution fluorescence intensity was measured at excitation wavelength was 415 nm and the emission wavelength range was 415–800 nm.

Selectivity and anti-interference ability

For the selectivity experiment, the concentration of all investigated interfering substances (AD, Trp, Cys, Tyr, His, Asp, Gly, Met, Lys, BAP, UA, GSH, SA, phenol, pyrocatechol, and NA) was 10 times higher than that of DA (20 μM). To test the anti-interference ability of the constructed sensing DA system, the effects of possible coexisting substances in the blood sample were investigated, such as AD, Trp, Cys, Tyr, His, Asp, Gly, Met, Lys, Glu, UA, GSH, Na^+, and AA. The other steps were consistent with the fluorescent methods for detecting DA (excitation wavelength at 415 nm and emission length at 488 nm).

Determination of DA in serum samples

The healthy human serum was taken and analyzed. The PBS buffer solution (pH = 7.1) was used to dilute the serum sample tenfold prior to the experiment. The samples were prepared for the spiking samples by adding standard DA solutions in a range of known concentrations. Three parallel experiments were carried out for each concentration of the DA sample solution, which had concentrations of 10 μM and 150 μM, respectively. A fluorescence spectrophotometer was used to record and plot the fluorescence spectra after the additional elements were added to the supernatants of the three concentrations and incubated for 20 min.

Results and discussion

Characterization

The preparation process of Fe_3O_4-MWCNTs@Hemin nanocomposites is shown in Scheme 1 and described in the Supporting Information. The TEM was used for investigating the size and morphology. As shown in Fig. 1a, the Fe_3O_4

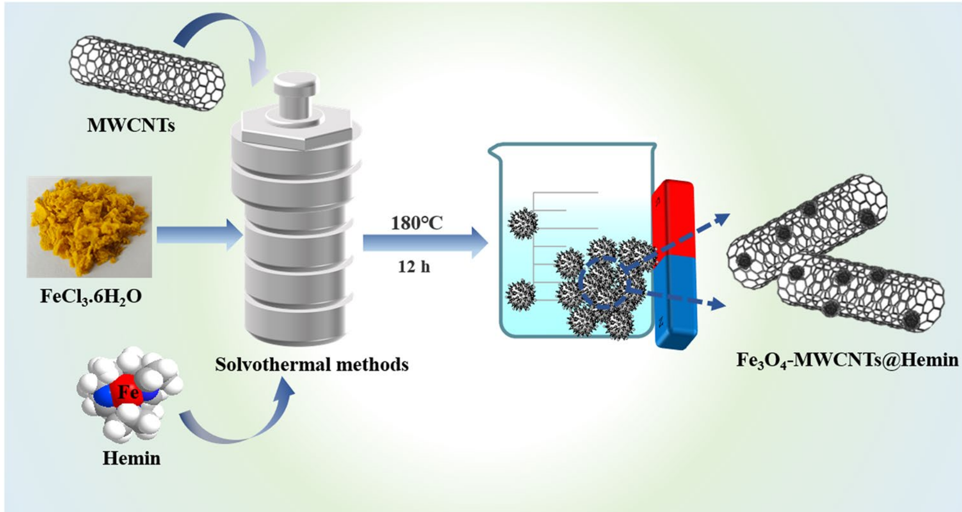

Scheme 1 Schematic illustration of the preparation of Fe_3O_4-MWCNTs@Hemin

displayed irregular spherical particles with a smooth surface of about 90 nm in diameter. The MWCNTs show curved and interlaced pipelines structure that could provide convenience for Fe_3O_4@Hemin adhesion (Fig. S1a–b). As shown in Fig. 1b, the Fe_3O_4@Hemin nanocomposites displayed a black, spherical shape with a rough surface, and a typical second-colored structure, which are attached to the surface of the MWCNTs [26]. The high-resolution TEM image (Fig. 1c) clearly depicted the interplanar distance between adjacent lattice fringes was measured at approximately 0.39 to 0.47 nm corresponding to the (111) plane of Fe_3O_4 nanoparticle [26–28]. As shown in Fig. 1d, Fe_3O_4 and hemin composite with diameters ranging from 140 to 205 nm were attached to the surface of the MWCNTs, the diameter increases significantly by comparing to the Fe_3O_4 nanocomposites. All of the results further suggested the successfully synthesized Fe_3O_4-MWCNTs@Hemin composites.

X-ray diffractogram (XRD) analysis was used to determine the structure and size of the crystal. Figure 1e illustrates the XRD pattern of the bare Fe_3O_4-MWCNT@Hemin nanohybrid. A typical graphitic carbon diffraction peak was observed in the image at $2\theta = 25.8°$, matching the (002) plane of MWCNTs, showing that the carbon structure of MWCNTs has remained intact after the functionalization by chemical processes of high temperature [29]. According to the JCPDS card No. 03–065-3107, the diffraction peaks at $2\theta = 30.4°$, 35.4°, 43.0°, 53.5°, 56.9°, and 62.6° correspond to (220), (311), (400), (422), (511), and (440) crystal plane of the standard XRD data correspond to the magnetite Fe_3O_4 crystal structure, respectively [27, 30]. Therefore, the Fe_3O_4-MWCNT@Hemin nanoparticles were synthesized successfully [26].

The XPS spectra of several catalytic layers were collected in order to better understand how MWCNTs contribute to the acceleration of Fe(II) regeneration. As shown in Fig. 1f and Table S1, the broad scan spectra and element mass ratio showed the existence of four elements (C, N, O, and Fe) in Fe_3O_4-MWCNT@Hemin. The N 1 s appeared in decorating with the hemin, which could prove the nanocomposites were synthesized successfully. Figure 1g shows the peak positions at 709.2 and 721.7 eV, which correspond to Fe $2p_{3/2}$ and Fe $2p_{1/2}$ species, the Fe $2p_{3/2}$ spectrum may be divided into two components of Fe^{2+} and Fe^{3+}. After the reaction, the peak of Fe^{2+} proportion is decreased, which indicated Fe^{2+} involved in Fenton reaction to generate ·OH. It shows that the increased POD-like activity is not caused by the produced iron atoms, but rather by the iron oxides. All the results suggest the successful construction of the Fe_3O_4-MWCNTs@Hemin. The FTIR spectrum of the as-prepared Fe_3O_4-MWCNTs@Hemin is depicted in Fig. S2. The peak at 590 cm^{-1} corresponds to the Fe–O stretching vibration band in Fe_3O_4. The carboxylic group's stretched vibration band, which was demonstrated in the previous research, was depicted as a peak about 1618 cm^{-1} in the hemin spectrum showing the C = C and C-H bonds on the protoporphyrin (IX) ring's stretching and bending vibration modes [29]. Additionally, the FTIR spectra of functionalized MWCNTs with carboxyl groups (COOH) group exhibit a broadening around 3413 cm^{-1}, which is related to the tensile strength O–H of the O = C-O, demonstrating that hemin interacts with hydroxyl groups on the surface of Fe_3O_4 through hydrogen bonding [24, 31]. These findings unambiguously showed that hemin molecules were effectively bonded to the surfaces of MWCNTs and Fe_3O_4.

As illustrated in Fig. S3, the distribution of Fe_3O_4-MWCNTs@Hemin in an aqueous solution is uniform in the absence of a magnetic field. However, when an external magnet was brought close by the highly dispersed Fe_3O_4-MWCNTs@Hemin in the aqueous solution quickly came together, indicating Fe_3O_4-MWCNTs@Hemin

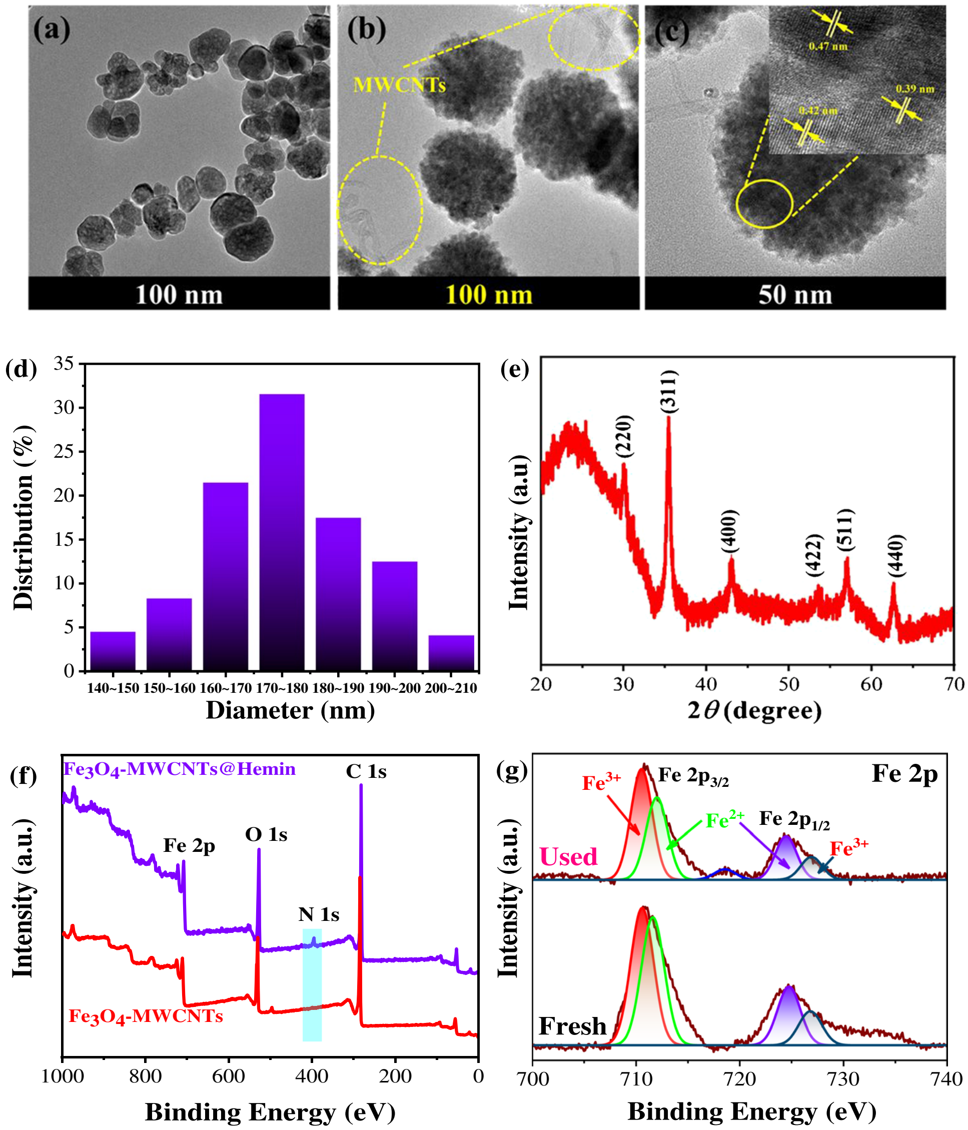

Fig. 1 **a** TEM of Fe_3O_4. **b** The TEM image. **c** HRTEM image and **d** size distribution of Fe_3O_4-MWCNTs@Hemin. **e** XRD spectrum of Fe_3O_4-MWCNTs@Hemin. XPS spectra of as-synthesized Fe_3O_4-MWCNTs@Hemin: **f** wide scan; **g** Fe 2p spectrum

nanocomposites could be recycled from aqueous solution easily due to the excellent magnetic property, which provides the convenience for detection.

POD-like activities

The oxidation performances of the mimic enzymes on the substrates TMB, OPD, ABTS, and DA were examined to analyze the POD-like activities of the mimetic enzymes in the activation of H_2O_2. As shown in Fig. 2a, in the presence of H_2O_2, Fe_3O_4-MWCNTs@Hemin catalyzed three kinds of substrate to produce different color changes of the reaction, and corresponding maximum absorption value center. Because of superb mimic enzyme activity, the DA was determined to evaluate POD-like activity of Fe_3O_4-MWCNTs@Hemin in the activation of H_2O_2. The UV–vis absorption spectra presented in Fig. 2b, it was concluded that Fe_3O_4-MWCNTs@Hemin could catalyze the oxidation of DA, the absorbance values of DA at 278 nm and oxidized DA (dopaquinone) at 392 nm.

Consequently, more research was done on the nanozyme Fe_3O_4-MWCNTs@Hemin's catalytic activity. Excess TMB and H_2O_2 substrate were present during the enzyme kinetic studies. The results show that the catalyzed reaction of Fe_3O_4-MWCNTs@Hemin obeys Michaelis–Menten equation. Michaelis constant (K_m) is deemed as the indicator of enzyme affinity to substrates and maximum initial velocity (V_{max}) was obtained from Lineweaver–Burk plot (Fig. 2c–d). The K_m and V_{max} value of Fe_3O_4-MWCNTs@Hemin with the substrate of TMB is 0.06 mM and 4.05×10^{-8} M·s^{-1}. As shown in Table S2, compared with other reported POD-like materials such as HRP, h-Fe_3O_4@ppy, Fe_3O_4@MnO_2, PA-Tb-Cu, and FeS_2 nanozymes, it is concluded that the

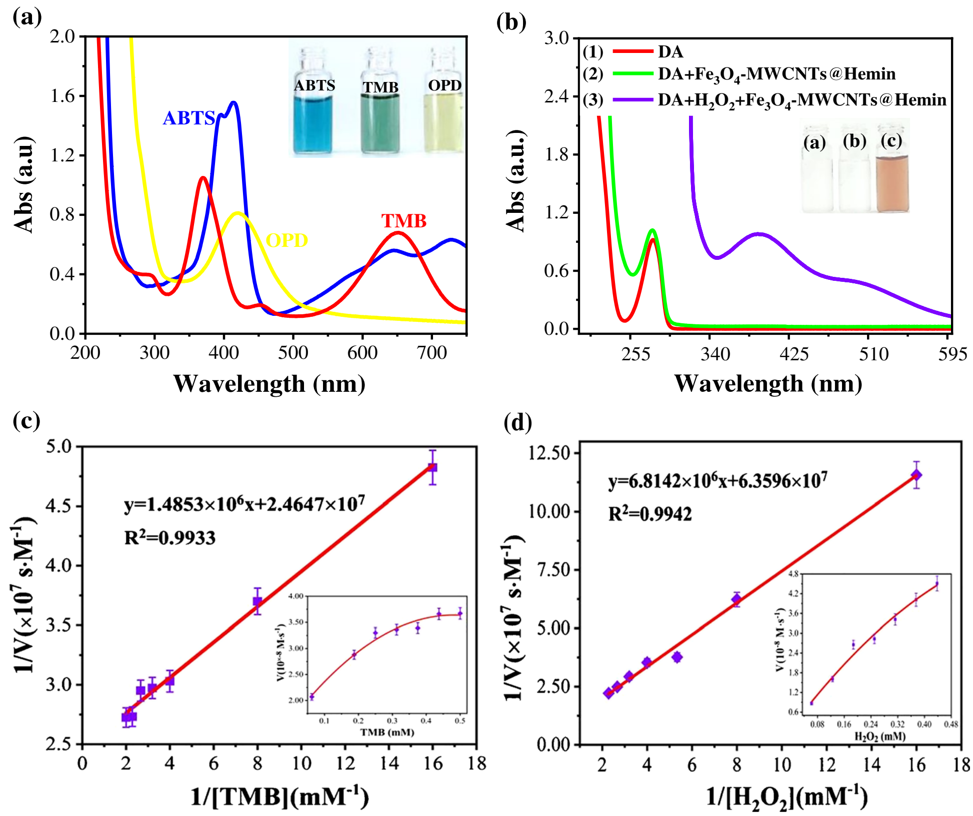

Fig. 2 **a** UV–vis absorption spectra of different substrates to verify the POD-like activity of Fe_3O_4@MWCNTs@Hemin. **b** UV–vis absorption spectra of DA substrate to verify the POD-like of Fe_3O_4@MWCNTs@Hemin. **c**, **d** Relationship of reaction rate and substrate concentration of the reaction of H_2O_2 catalyzed by Fe_3O_4@MWCNTs@Hemin nanozyme and corresponding Lineweaver–Burk plot

synthesized Fe_3O_4-MWCNTs@Hemin was lower K_m than that of the frequently used horseradish HRP, suggesting that Fe_3O_4-MWCNTs@Hemin has a higher affinity to H_2O_2 than HRP. Meanwhile, the maximum reaction rate of Fe_3O_4-MWCNTs@Hemin for substrate H_2O_2 was approximately higher than that of HRP, indicating a higher excellent catalytic activity of Fe_3O_4-MWCNTs@Hemin. Interestingly, two frequently used components of MWCNTs and hemin were used for enhancing the Fe_3O_4 POD-like activities, which is the most obvious difference reported in other Fe_3O_4 literature. Unlike most of the structures, most nanozymes have oxidized popular substrate such as TMB, ABTS, and OPD for the detection. The Fe_3O_4-MWCNTs@Hemin catalyzed the oxidation reaction of different substrates including DA in the presence of H_2O_2. In addition, the derivative reaction process can be achieved with the oxidation process by one-step methods.

Sensing of DA

To evaluate the POD-like capability of Fe_3O_4-MWCNTs@Hemin nanozyme for using DA as the target object, the reaction process is demonstrated in Fig. 3a. As shown in Fig. 3b, the UV absorption of the DA oxidation products at 392 nm can be attributed to the conjugated C = O units of the newly formed dopaquinone, which is different from DA. The UV absorption was shifted to 450 nm when the β-NAP was added and formed more conjugated system. Figure 3c shows the fluorescence spectra of Fe_3O_4-MWCNTs@Hemin catalyzing DA solution under various conditions. The results show that in the absence of Fe_3O_4-MWCNTs@Hemin, no obvious fluorescence was observed in the system. In the presence of Fe_3O_4-MWCNTs@Hemin, nanozyme consequently coupled with the homologous catechol derivatives *o*-quinone intermediate. Subsequently, β-NAP was reacted with *o*-quinone and regarded as tracer material for coming into being fluorescent signals fleetly. According to Fig. S4, the DA detection system displays a strongly fluorescence emission excitation wavelength at 415 nm and a significant fluorescence emission peak at 488 nm. The fluorescence intensity rose with the addition of DA to the entire mixture. By measuring the fluorescence intensity of the combination, these results show that quantitative detection of DA is possible. As for nanometer material, after the addition of Fe_3O_4 and Fe_3O_4-MWCNTs, the solution became weakly fluorescent (Fig. S5), which shows Fe_3O_4 and Fe_3O_4-MWCNTs had no certain catalytic activity for the reaction of DA and β-NAP. In the presence of Fe_3O_4-MWCNTs@Hemin in the solution, the fluorescence intensity of the solution of DA and β-NAP was enhanced immediately.

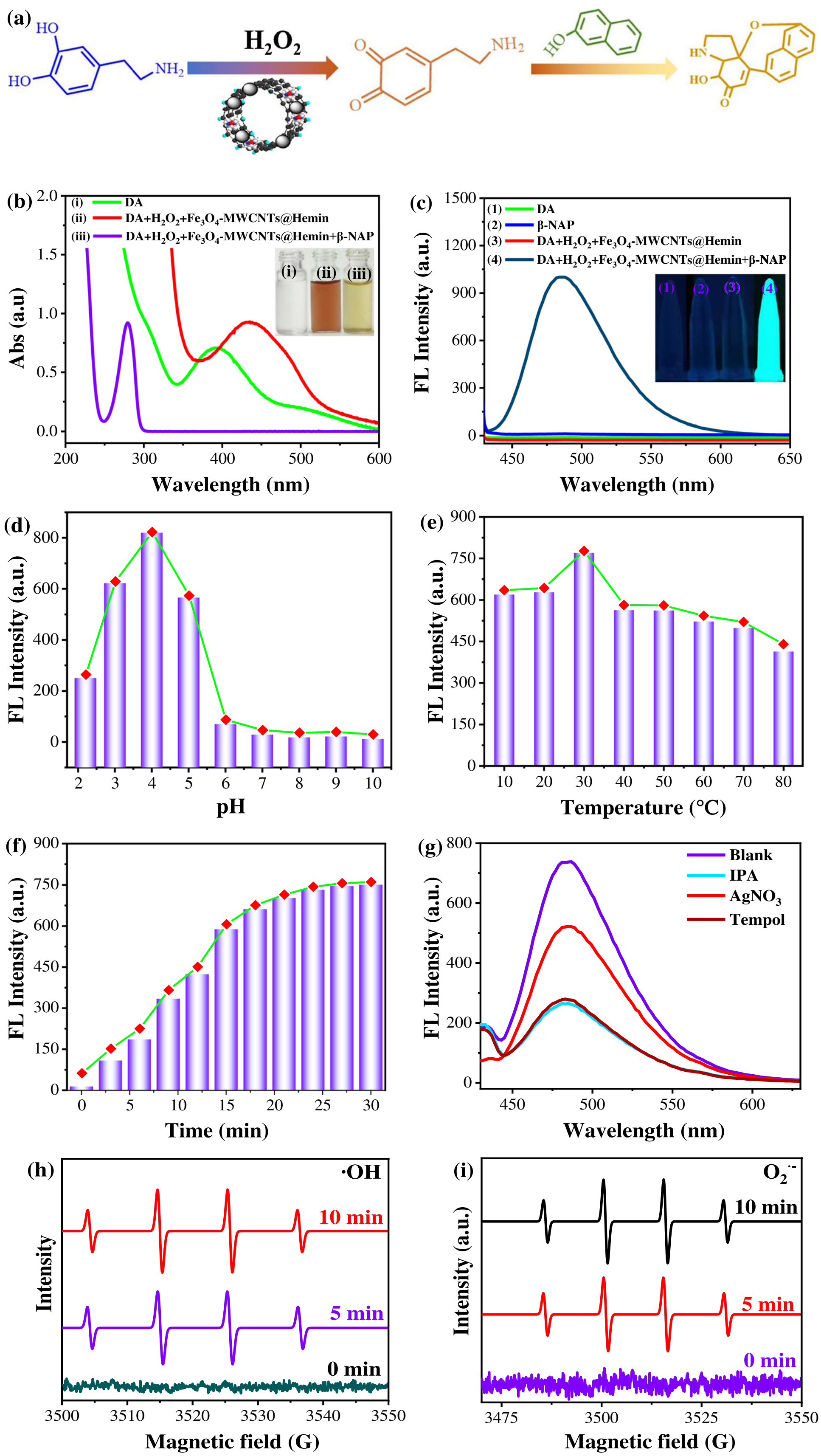
(a)
HO
HO
NH2
H2O2
O
O
NH2
HO
HN
HO
O
O
(b)
(i) DA
(ii) DA+H2O2+Fe3O4-MWCNTs@Hemin
(iii) DA+H2O2+Fe3O4-MWCNTs@Hemin+β-NAP
(i) (ii) (iii)
Abs (a.u)
Wavelength (nm)
(c)
(1) DA
(2) β-NAP
(3) DA+H2O2+Fe3O4-MWCNTs@Hemin
(4) DA+H2O2+Fe3O4-MWCNTs@Hemin+β-NAP
(1) (2) (3) (4)
FL Intensity (a.u.)
Wavelength (nm)
(d)
FL Intensity (a.u.)
pH
(e)
FL Intensity (a.u.)
Temperature (°C)
(f)
FL Intensity (a.u.)
Time (min)
(g)
Blank
IPA
AgNO3
Tempol
FL Intensity (a.u.)
Wavelength (nm)
(h)
·OH
10 min
5 min
0 min
Intensity
Magnetic field (G)
(i)
O2·−
10 min
5 min
0 min
Intensity (a.u.)
Magnetic field (G)

◂**Fig. 3** **a** The oxidation reaction of DA and reacted with β-NAP. **b** UV–vis absorption spectra of different reaction DA systems: (1) DA, (2) DA+H_2O_2+Fe_3O_4-MWCNTs@Hemin, (3) DA+H_2O_2+Fe_3O_4-MWCNTs@Hemin, (4) DA+H_2O_2+Fe_3O_4-MWCNTs@Hemin+β-NAP. **c** Fluorescence spectra of DA system in the presence of H_2O_2, Fe_3O_4-MWCNTs@Hemin, and β-NAP. Effect of pH **d**, temperature **e**, and reaction time **f** on the fluorescence intensity of the sensing DA system; **g** free radical capture for catalysis mechanism. **h**, **i** ESR spectrum for detection of the ·OH and $O_2^{\bullet-}$ generation

Optimization of experimental condition

The generated Fe_3O_4-MWCNTs@Hemin nanozymes catalytic activity was substantially influenced by pH, temperature, and time just as natural POD and other POD mimics based on nanomaterials. The nanozyme displayed high catalytic activity over a broad pH range from 2.2 to 4.0, and the optimal pH value for Fe_3O_4-MWCNTs@Hemin nanozyme was found to be 4.0, as shown in Fig. 3d. The activity of the nanozyme increased dramatically from pH 3.0 to 5.0, while it significantly decreased above pH = 6.0. The catalytic activity of these nanozymes increased from 4 to 30°C and then dramatically decreased from 30 to 80°C, as shown in Fig. 3e. The POD-like activity of Fe_3O_4-MWCNTs@Hemin nanozyme was still barely alive when the temperature reached 80°C. Fe_3O_4-MWCNTs@Hemin exhibited high catalytic activity during the reaction time from 0 to 30 min, while the activity of POD increased with increasing reaction time from 0 to 20 min (Fig. 3f).

The capturing experiments were further studied to verify the generation of the radical species during the POD-like activity of Fe_3O_4@MWCNTs@Hemin. During the catalytic reaction for detecting important active species in the presence of nanozyme catalysis mechanism is investigated with 2,2,6,6-tetramethyl-1-piperidinyloxy (Tempol) for $\bullet O_2^-$ scavengers, isopropanol (IPA) for •OH scavengers, and $AgNO_3$ as e^- scavengers, respectively. As shown in Fig. 3g, a significant decrease in the fluorescence intensity of the system can be observed after the addition of IPA and Tempol to the DA solution, which indicates that the most dominant radical in the Fe_3O_4-MWCNTs@Hemin-catalyzed oxidation of DA system is •OH and $O_2^{\bullet-}$. To further confirm the result, the ESR spectrum was selected to study the involving ·OH and $O_2^{\bullet-}$. DMPO was used to track the formation of ·OH in the reaction system (Fig. 3h). In the presence of Fe_3O_4-MWCNTs@Hemin, the signal strength gradually increases over time, which indicates that ·OH is generated in the reaction system. The peroxidase-like property of Fe_3O_4-MWCNTs@Hemin could further catalyze the oxidation of H_2O_2 to ·OH. Meanwhile, DMPO was also used to track the $O_2^{\bullet-}$. As illustrated in Fig. 3i, the peak signal was detected for different time periods, which indicates that substantial $O_2^{\bullet-}$ was generated by decomposing oxygen in the presence of Fe_3O_4-MWCNTs@Hemin. Consequently, two kinds of ROS can be generated and function in the presence of nanozyme.

Evaluation of the developed method for DA detection

Under the ideal detecting circumstances, the nanozyme reaction to DA at various concentrations is shown in Fig. 4a–b. It was discovered that when the DA concentration increased, the fluorescence intensity steadily increased. In the low concentration range (0.33 up to 106 μM), there was a strong linear association ($y = 6.646x + 16.546$, $R^2 = 0.992$). By using the formula $3\sigma/K_{sv}$ (where 3 is the factor of 99% confidence level, δ is the standard deviation of 20 blank experiments, K_{sv} is the slope of the linear regression equation), the limit of detection (LOD) was determined. The LOD was calculated to be 0.14 μM in accordance with the equation. The low LOD value suggested Fe_3O_4-MWCNTs@Hemin was a sensitive fluorescence sensor with the potential to detect DA in other blood systems. Comparing the detection ranges and LODs of other approaches, the approach we proposed has displayed high specificity, sensitivity, and low detection limit for the DA determination (Table S3). However, the fluorescence platform is based on the oxidation reaction, the strong reducibility matter has a strong influence on the detection. It is important to note that some foods have considerable reducibility properties, which is difficult for detecting for DA in these foods.

Selectivity and anti-interference test of the DA system

The reaction of additional compounds, such as amino acids (including Trp, Cys, Tyr, His, Asp, Gly, Met, and Lys), BPA, UA, GSH, SA, phenol, and pyrocatechol, was examined to look into the selectivity of the fluorescent platform. According to Fig. 4c, the only DA showed a significant increase in fluorescence intensity at 488 nm under excitation length at 415 nm, which indicates a high selectivity of this DA detection method.

In order to illustrate the possibility of using this method for DA determination in actual blood samples, the anti-interferences such as other amino acids and phenols were added to the Fe_3O_4-MWCNTs@Hemin + H_2O_2 + DA + β-NAP system, and the changes of absorbance were observed (Fig. 4d). Even though they were at 10 times larger concentrations than the 200 μM different kinds of compounds that the system

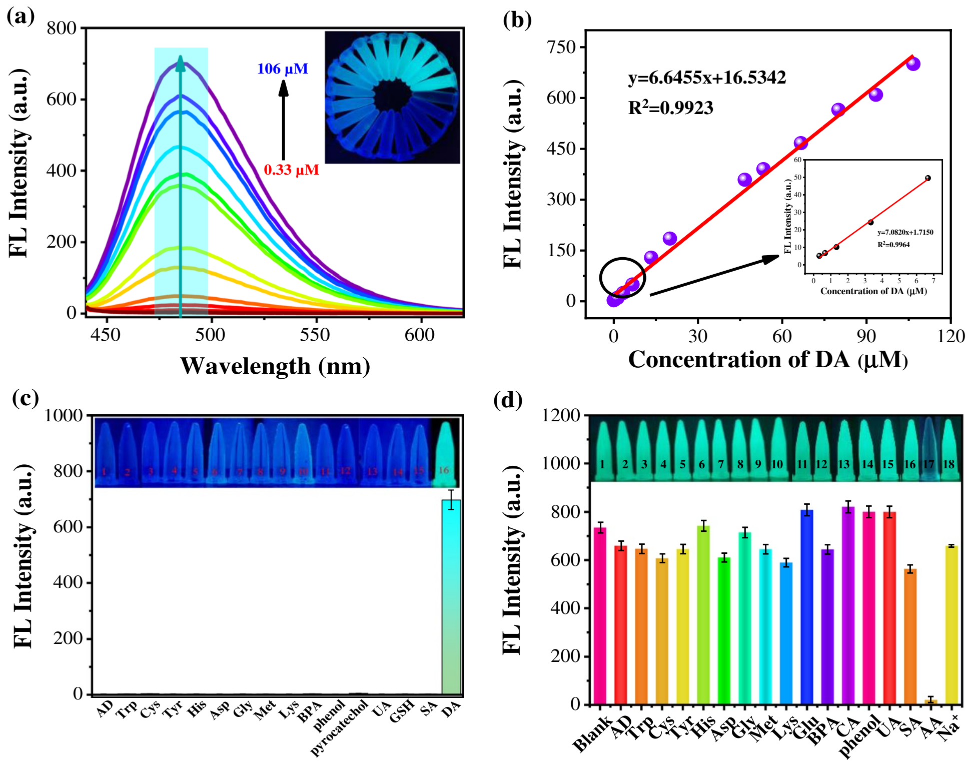

Fig. 4 **a** Fluorescence emission spectra of Fe_3O_4-MWCNTs@Hemin solutions with DA concentrations varying from 0.33 to 106 μM. **b** Fluorescence intensity DA concentration calibration curve. Inset: enlarged graph of part of the calibration curve. **c** Specificity test of the fluorescence method based on Fe_3O_4-MWCNTs@Hemin as POD-like mimics for detection of DA in the activation of H_2O_2. **d** Interference study of DA detection, the concentration of DA is 20 μM, and the concentration of the interference element is 200 μM (all of these solution fluorescence intensities were measured with excitation at 415 nm and emission length at 488 nm)

fluorescence intensity was slightly altered at 488 nm. The fluorescent probes exhibit great selectivity and sensitivity to DA response, according to these data. Nonetheless, AA demonstrated clear interfering effects, which may be efficiently avoided by adding masking agent AAQ-2 [32]. Meanwhile, the AA concentration of blood sample is less than 10 mg/L, which is considerably lower than the experimental anti-inference contents. Generally, these results indicate the high anti-interference ability of the detection DA.

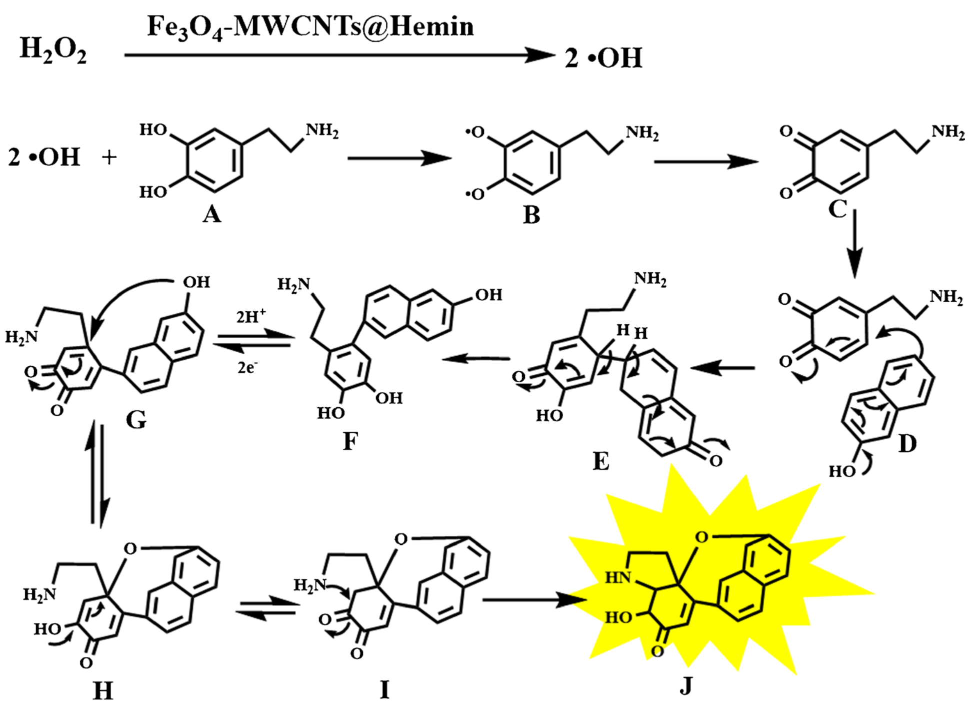

Scheme 2 Plausible mechanism of the reaction of DA with β-NAP

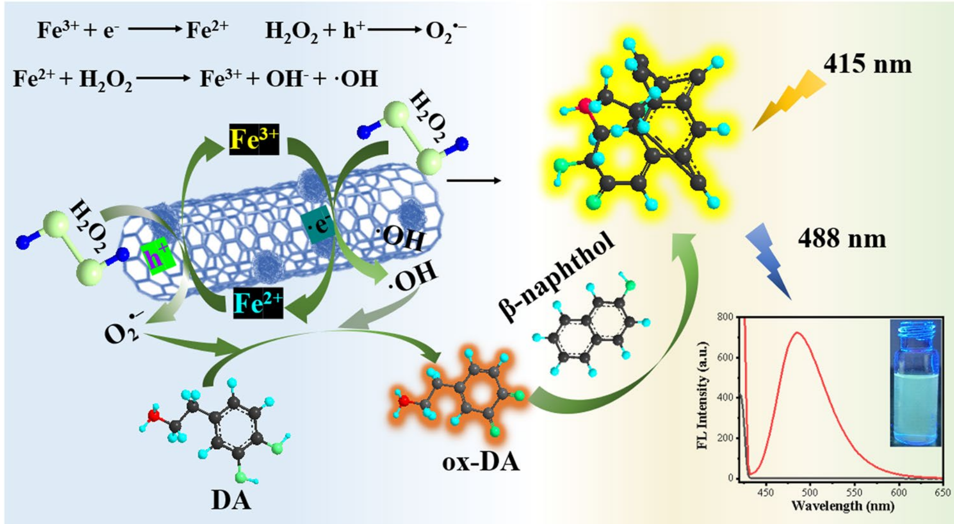

Scheme 3 Illustration of detecting DA by Fe_3O_4-MWCNTs@Hemin with the fluorescence methods

Mechanism investigation

Based on the capturing experiments and ESR results, the •OH and $O_2^{\bullet-}$ plays a significant role in catalyze reaction of the oxidation DA mechanism of Fe_3O_4@MWCNTs@Hemin. As indicated in Scheme 2, it is claimed that Fe_3O_4@MWCNTs@Hemin could resolve H_2O_2 to generate •OH, then DA (**A**) was oxidized and formed intermediate formation (**B**), then **B** is further formed to dopaquinone (**C**), undergo intermolecular Michael addition reaction by β-NAP (**D**) to give intermediate (**E**) under acid environment. **F** was obtained by the **E** intramolecular rearrangement. **F** contains a DA diphenol structure, Fe_3O_4-MWCNTs@Hemin could oxidize and dehydrogenated **F** again to obtain **G**. The lone electron of -OH would attack **G** and undergo intramolecular cyclization to obtain **H**. The intermediate **I** has the enol structure, which would form a carbonyl group, and the carbonyl group in the molecule would be attacked by the amine's lone electron, resulting in the final chromo-fluorophore product **J**. Fig. S6 presents the ^{1}H-NMR (C_5D_5N, 600 MHz) and ^{13}C-NMR (C_5D_5N, 150 MHz) spectra of the fluorescence product. The ^{13}C signal within 170–190 ppm belongs to the carbonyl carbon, 100–175 ppm are assigned to the aromatic carbons, and those below 100 ppm are attributed to the aliphatic carbons. All the carbons are consistently matched with the fluorescence derivative structure, and the result confirms that final products structure was same with the Scheme 2J.

Fe^{2+} is more active in the Fenton process, the Fe^{2+} species could rapidly react with H_2O_2 to produce abundant •OH and Fe^{3+} [33]. As shown in Scheme 3, Fe^{3+}/Fe^{2+} redox couples promote the generation of •OH and $O_2^{\bullet-}$. In addition, DA was oxidized to dopaquinone by the ROS from Fe_3O_4@MWCNTs@Hemin under in presence of H_2O_2 conditions. After that, adding β-NAP to react with the intermediate, which the fluorescence product was created by the reaction [34].

DA detection in human serum samples

Human blood samples spiked with various doses of DA were subjected to the proposed Fe_3O_4@MWCNTs@Hemin technique to quantify DA concentrations. According to Table 1 summary of the methods, recovery rates range from 81.3 to 96.7%, and RSD is less than 5%. The Fe_3O_4-MWCNTs@Hemin technique was successful in detecting the micromolar level DA in intricate biological samples.

Table 1 Determination of DA in human serum samples

Sample	DA added (μM)	DA found (μM)	Recovery (%)	RSD (%), $n=3$
	0	1.2 ± 0.06	-	-
1	10	10.0 ± 0.12	87.6	1.4
	150	145.9 ± 0.32	96.4	3.3
2	0	1.4 ± 0.17	-	-
	10	9.6 ± 0.25	81.3	4.2
	150	146.5 ± 0.52	96.7	2.5

Conclusions

In the research work, the MWCNTs-modified Fe_3O_4-Hemin nanozymes were successfully synthesized by hydrothermal method. Hemin could improve the Fe_3O_4 catalytic activities and MWCNTs can provide make more active sites available for the substrate binding. The experimental results demonstrated that Fe_3O_4-MWCNTs@Hemin has outstanding POD-like activity due to unique design and the interaction of various components. The magnetic nanozymes catalyzed the H_2O_2 to convert a large number of ·OH and $O_2^{\cdot-}$, which was effective to oxidize variety of substrates such as TMB, OPD, ABTS, and dopamine. Meanwhile, the oxidation products were reacted with β-NAP and producing strong fluorescence, which excitation wavelength at 415 nm and emission wavelength at 488 nm and the fluorescence intensity was linearly with the concentration of DA. The fluorescence detection platform was applied to detect DA in blood sample and the standard recovery rate in the range of 81.3–96.7%. The sensor shows highly selectivity and sensitivity, which is expected to apply to detect DA in blood sample in future.

Supplementary information The online version contains supplementary material available at https://doi.org/10.1007/s00604-023-05796-x.

Funding This work was supported by the Analysis and Testing Foundation of Kunming University of Science and Technology (grant numbers 2021T20200097 and 2021M20202118090).

Data Availability Data will be made available on request.

Declarations

Ethical standards This research was approved by the Kunming University of Science and Technology Ethic Committee (KMUST-MEC-087), and all experiments were performed in accordance with the Guideline for Experimentation of Kunming University of Science and Technology.

Source of biological material The blood samples were collected from volunteers who gave informed written consent for inclusion.

Competing interests The authors declare no competing interests.

References

1. Wan Y, Li L, Jiang M, Yang X, Yu X, Xu L (2022) One-pot synthesis of boron and nitrogen co-doped silicon-carbon dots for fluorescence enhancement and on-site colorimetric detection of dopamine with high selectivity. Appl Surf Sci. 573:151457. https://doi.org/10.1016/j.apsusc.2021.151457
2. Tang X, Liu Y, Bai X, Yuan H, Hu Y, Yu X, Liao X (2021) Turn-on fluorescent probe for dopamine detection in solutions and live cells based on in situ formation of aminosilane-functionalized carbon dots. Anal Chim. Acta. 1157:338394. https://doi.org/10.1016/j.aca.2021.338394
3. Wang Y, Wang D, Dong S, Qiao J, Zeng Z, Shao S (2022) A visible-light-driven photoelectrochemical sensing platform based on the $BiVO_4$/FeOOH photoanode for dopamine detection. Electrochim. Acta. 414:140207. https://doi.org/10.1016/j.electacta.2022.140207
4. Lv Q, Chen L, Liu H, Zou L (2022) Peony-like 3D-MoS_2/graphene nanostructures with enhanced mimic peroxidase performance for colorimetric determination of dopamine. Talanta 247:123553. https://doi.org/10.1016/j.talanta.2022.123553
5. Guo H, Liu B, Pan Z, Sun L, Peng L, Chen Y, Wu N, Wang M, Yang W (2022) Electrochemical determination of dopamine and uric acid with covalent organic frameworks and Ox-MWCNT co-modified glassy carbon electrode. Colloids Surf. 648:129316. https://doi.org/10.1016/j.colsurfa.2022.129316
6. Zhao H, Mu H, Bai Y, Yu H, Hu Y (2011) A rapid method for the determination of dopamine in porcine muscle by pre-column derivatization and HPLC with fluorescence detection. J Pharm Anal 1(3):208–212. https://doi.org/10.1016/j.jpha.2011.04.003
7. Gottås A, Ripel A, Boix F, Vindenes V, Mørland J, øiestad EL, (2015) Determination of dopamine concentrations in brain extracellular fluid using microdialysis with short sampling intervals, analyzed by ultra high performance liquid chromatography tandem mass spectrometry. J Pharmacol Toxicol Methods 74:75–79. https://doi.org/10.1016/j.vascn.2015.06.002
8. Zhang Y, Yin H, Jia C, Dong Y, Ding H, Chu X (2020) Electrogenerated chemiluminescence of $Ru(bpy)_3^{2+}$ at MoS_2 nanosheets modified electrode and its application in the sensitive detection of dopamine. Spectrochim. Acta, Part A 240:118607. https://doi.org/10.1016/j.saa.2020.118607
9. Sun Y, Cheng Y, Yin X (2021) Dual-ligand lanthanide metal-organic framework for sensitive ratiometric fluorescence detection of hypochlorous acid. Anal Chem 93(7):3559–3566. https://doi.org/10.1021/acs.analchem.0c05040
10. Chen B, Chang S, Lv J, Qian R, Li D (2021) Temperature-modulated porous gadolinium micro-networks with hyperchrome-enhanced fluorescence effect. Chem Eng. J. 422:129959. https://doi.org/10.1016/j.cej.2021.129959
11. He Y, Pan C, Cao H, Yue M, Wang L, Liang G (2018) Highly sensitive and selective dual-emission ratiometric fluorescence detection of dopamine based on carbon dots-gold nanoclusters hybrid. Sens Actuators, B 265:371–377
12. Liu X, Yu W, Mu X, Zhang W, Wang X, Gu Q (2023) A fluorescence probe based on carbon dots for determination of dopamine utilizing its self-polymerization. Spectrochim Acta, Part A 287(2):122112
13. Xu S, Chang L, Zhao X, Hu Y, Lin Y, Chen Z, Ren X, Mei X (2022) Preparation of epigallocatechin gallate decorated Au-Ag nano-heterostructures as NIR-sensitive nano-enzymes for the treatment of osteoarthritis through mitochondrial repair and cartilage protection. Acta Biomater 144:168–182. https://doi.org/10.1016/j.actbio.2022.03.038
14. Gao L, Zhuang J, Nie L, Zhang J, Zhang Y, Gu N, Wang T, Feng J, Yang D, Oerrett S (2007) Intrinsic peroxidase-like activity of ferromagnetic nanoparticles. Nat. Nanotechnol. 2:577–583. https://doi.org/10.1038/nnano.2007.260
15. Yang W, Fei J, Xu W, Jiang H, Sakran M, Hong J, Zhu W, Zhou X (2022) A biosensor based on the biomimetic oxidase Fe_3O_4@MnO_2 for colorimetric determination of uric acid. Colloids Surf, B 212:112347–112347. https://doi.org/10.1016/j.colsurfb.2022.112347
16. Liu H, Xu H, Zhu L, Wen J, Qiu Y, Gu C, Li L (2021) Colorimetric detection of hydrogen peroxide and glutathione based on peroxidase mimetic activity of fe_3o_4-sodium lignosulfonate nanoparticles. Chinese J Anal Chem 49(9):21160–21169. https://doi.org/10.1016/S1872-2040(21)60113-5
17. Nejad FG, Sheikhshoaie I, Beitollahi H (2022) Simultaneous detection of carmoisine and tartrazine in food samples using GO-Fe_3O_4-PAMAM and ionic liquid based electrochemical sensor. Food Chem Toxicol 162:112864. https://doi.org/10.1016/j.fct.2022.112864

18. Li S, Pang C, Ma X, Wu Y, Wang M, Xu Z, Luo J (2022) Aggregation-induced electrochemiluminescence and molecularly imprinted polymer based sensor with Fe_3O_4@Pt nanoparticle amplification for ultrasensitive ciprofloxacin detection. Microchem. J. 178:107345. https://doi.org/10.1016/j.microc.2022.107345
19. Liu W, Chu L, Zhang C, Ni P, Jiang Y, Wang B, Lu Y, Chen C (2021) Hemin-assisted synthesis of peroxidase-like Fe-N-C nanozymes for detection of ascorbic acid-generating bio-enzymes. Chem Eng. J. 415:128876. https://doi.org/10.1016/j.cej.2021.128876
20. Zhang F, Long X, Zhang D, Sun Y, Zhou Y, Ma Y, Qi L, Zhang X (2014) Layered double hydroxide-hemin nanocomposite as mimetic peroxidase and its application in sensing. Sens Actuators, B 192:150–156. https://doi.org/10.1016/j.snb.2013.10.097
21. Li D, Wu S, Wang F, Jia S, Liu Y, Han X, Zhang L, Zhang S, Wu Y (2016) A facile one-pot synthesis of hemin/ZIF-8 composite as mimetic peroxidase. Mater Lett 178:48–51. https://doi.org/10.1016/j.matlet.2016.04.200
22. Sun R, Wang Y, Ni Y, Kokot S (2014) Spectrophotometric analysis of phenols, which involves a hemin–graphene hybrid nanoparticles with peroxidase-like activity. J Hazard Mater 266:60–67. https://doi.org/10.1016/j.jhazmat.2013.12.006
23. Liu H, Jin F, Liu D, Liu W, Zhao J, Chen P, Wang Q, Wang X, Zou Y (2022) Preparation and electrochemical performance of MWCNT/MoS_2 composite modified Co–P hydrogen storage material. Solid State Sci. 131:106952. https://doi.org/10.1016/j.solidstatesciences.2022.106952
24. Mousaabadi KZ, Ensafi AA, Rezaei B (2022) Simultaneous determination of some opioid drugs using Cu-hemin MOF@MWCNTs as an electrochemical sensor. Chemosphere 303:135149. https://doi.org/10.1016/j.chemosphere.2022.134023
25. Tong Y, Boldoo T, Ham J, Redcho HC (2020) Improvement of photo-thermal energy conversion performance of MWCNT/Fe_3O_4 hybrid nanofluid compared to Fe_3O_4 nanofluid. Energy. 196:117086. https://doi.org/10.1016/j.energy.2020.117086
26. Cui L, Huang H, Ding P, Zhu S, Jing W, Gu X (2020) Cogeneration of H_2O_2 and ·OH via a novel Fe_3O_4/MWCNTs composite cathode in a dual-compartment electro-Fenton membrane reactor. Sep Purif Technol. 237:116380. https://doi.org/10.1016/j.seppur.2019.116380
27. Hussain S, Alam MM, Imran M, Ali MA, Ahamad T, Haidyrah AS, Alotaibi SMAR, Naik M, Shariq M (2022) A facile low-cost scheme for highly photoactive Fe_3O_4-MWCNTs nanocomposite material for degradation of methylene blue. Alexandria Eng J 61:9107–9117. https://doi.org/10.1016/j.aej.2022.02.050
28. Shamsazar A, Asadi A, Seifzadeh D, Mahdavi M (2021) A novel and highly sensitive sandwich-type immunosensor for prostate-specific antigen detection based on MWCNTs-Fe_3O_4 nanocomposite. Sens Actuators B. 346:130459. https://doi.org/10.1016/j.snb.2021.130459
29. Gharibshahi R, Omidkhah M, Jafari A, Fakhroueian Z (2020) Hybridization of superparamagnetic Fe_3O_4 nanoparticles with MWCNTs and effect of surface modification on electromagnetic heating process efficiency: a microfluidics enhanced oil recovery study. Fuel. 282:118603. https://doi.org/10.1016/j.fuel.2020.118603
30. Moghadam MTT, Seifi M, Askari MB, Azizi S (2022) ZnO-MWCNT@Fe_3O_4 as a novel catalyst for methanol and ethanol oxidation. J Phys Chem Solids. 165:110688. https://doi.org/10.1016/j.jpcs.2022.110688
31. Zhang Y, Wu P, Chen Z, Zhou L, Zhao Y, Lai Y, Duan Y, Wang F, Li S (2019) Synergistic effect in heterogeneous Fenton degradation of tetrabromobisphenol A by MWCNT and β-CD co-modified Fe_3O_4. Mater Res Bull 113:14–24. https://doi.org/10.1016/j.materresbull.2019.01.008
32. Yang J, Zhai X, Dong X, Zhao L, Zhang Y, Xiao H, Ju P, Duan J, Tang X, Hou B (2023) Peroxidase-like phosphate hydrate nanosheets bio-synthesized by a marine Shewanella algae strain for highly sensitive dopamine detection. Colloids Surf, B 225:113248. https://doi.org/10.1016/j.colsurfb.2023.113248
33. Huang X, Zhou H, Yue X, Ran S, Zhu J (2021) Novel magnetic Fe_3O_4/α-FeOOH nanocomposites and their enhanced mechanism for tetracycline hydrochloride removal in the visible photo-Fenton process. ACS Omega 6(13):9095–9103. https://doi.org/10.1021/acsomega.1c00204
34. Zhang D, Du P, Chen J, Guo H, Lu X (2021) Pyrazolate-based porphyrinic metal-organic frameworks as catechol oxidase mimic enzyme for fluorescent and colorimetric dual-mode detection of dopamine with high sensitivity and specificity. Sens Actuators, B 341:130000. https://doi.org/10.1016/j.snb.2021.130000

Publisher's note Springer Nature remains neutral with regard to jurisdictional claims in published maps and institutional affiliations.